Journal of Pharmaceutical Analysis 12 (2022) 801–807

Contents lists available at ScienceDirect

Journal of Pharmaceutical Analysis

journal homepage: www.elsevier.com/locate/jpa

Original article

Fluorescent intracellular imaging of reactive oxygen species and pH levels moderated by a hydrogenase mimic in living cells

Xin-Yuan Hu [a], Jia-Jing Li [a], Zi-Wei Yang [a], Jun Zhang [b, *], Huai-Song Wang [a, **]

[a] Department of Pharmaceutical Analysis, China Pharmaceutical University, Nanjing, 210009, China
[b] College of Food Science and Bioengineering, Tianjin Agricultural University, Tianjin, 300392, China

ARTICLE INFO

Article history:
Received 22 November 2021
Received in revised form
12 May 2022
Accepted 22 May 2022
Available online 28 May 2022

Keywords:
Cell imaging
[FeFe]-hydrogenase
Reactive oxygen species
Photocatalytic system

ABSTRACT

The catalytic generation of H_2 in living cells provides a method for antioxidant therapy. In this study, an [FeFe]-hydrogenase mimic [Ru + Fe_2S_2@F127(80)] was synthesized by self-assembling polymeric pluronic F-127, catalytic [Fe_2S_2] sites, and photosensitizer $Ru(bpy)_3^{2+}$. Under blue light irradiation, hydrated protons were photochemically reduced to H_2, which increased the local pH in living cells (HeLa cells). The generated H_2 was subsequently used as an antioxidant to decrease reactive oxygen species (ROS) levels in living cells (HEK 293T, HepG2, MCF-7, and HeLa cells). Our findings revealed that the proliferation of HEK 293T cells increased by a factor of about six times, relative to that of other cells (HepG2, MCF-7, and HeLa cells). Intracellular ROS and pH levels were then monitored using fluorescent cell imaging. Our study showed that cell imaging can be used to evaluate the ability of Ru + Fe_2S_2@F127 to eliminate oxidative stress and prevent ROS-related diseases.

1. Introduction

Reactive oxygen species (ROS), including O_2^{-}, hydroxyl radicals (·OH), and H_2O_2, play significant roles in regulating physiological activities. In healthy living cells, ROS are maintained at low levels. Abnormal overproduction of ROS is implicated in oxidative stress, which is associated with various diseases such as cancer, cardiovascular diseases, and neurological disorders [1–3]. Recent research has demonstrated that hydrogen (H_2) functions as an effective antioxidant and can be used as a therapeutic medical gas in the clinic [4–6]. Furthermore, H_2 not only reacts with·OH and peroxynitrite ($ONOO^{-}$), but also reduces cell apoptosis [7–9]. As an alternative to H_2, H_2-rich saline is suitable for clinical application in the treatment of ischemia-reperfusion injury [10], Alzheimer's and Parkinson's diseases [11], acute pancreatitis [12], and other oxidative stress-related diseases [13].

[FeFe]-hydrogenase ([FeFe]-H_2ase), a metalloenzyme extracted from green algae, is an effective biocatalyst for reducing hydrated protons to molecular H_2 [14]. Mimics of the [FeFe]-H_2ase active center, a [Fe_2S_2] cluster, have shown promise as catalysts for hydrated proton reduction. In particular, H_2 generation can be dramatically enhanced via artificial photocatalytic systems by combining [FeFe]-H_2ase mimics with photosensitizers (PSs) [15–17]. Since the first photocatalytic system was synthesized by Sun and co-workers in 2003 [18], similar artificial systems have been designed to produce H_2 under visible light irradiation. [Fe_2S_2] cluster-based photocatalytic systems are generally prepared by the following two methods: 1) linking PS to the active center of [FeFe]-H_2ase, and 2) incorporating [FeFe]-H_2ase mimics into self-assembling systems containing PS [19–21]. Briefly, photoinduced electron transfer from PS to the [Fe_2S_2] cluster is important for photocatalytic H_2 production.

Herein, we propose an [Fe_2S_2] cluster-based nanoarchitecture as an [FeFe]-H_2ase mimic for antioxidant H_2 photogeneration therapy. The nanoarchitecture was self-assembled from biologically inert pluronic F-127, [Fe_2S_2] cluster, and PS [$Ru(bpy)_3^{2+}$] (Fig. 1). Pluronic F-127 is a triblock copolymer that contains a central poly(propylene oxide) (PPO) block flanked by two poly(ethylene oxide) (PEO) units. Self-assembled spherical pluronic F-127 micelles have good biocompatibility, making them excellent candidates for drug carriers [22,23]. The [Fe_2S_2] clusters and $Ru(bpy)_3^{2+}$ were loaded into spherical pluronic F-127 micelles. This self-assembled system (Ru + Fe_2S_2@F127) was capable of photochemically generating H_2 under visible-light irradiation.

Overconsumption of oxygen in tumor tissues or inflammatory sites can lead to an acidic environment. Endosomes or lysosomes in

Peer review under responsibility of Xi'an Jiaotong University.
* Corresponding author.
** Corresponding author.
E-mail addresses: zjaiwa@163.com (J. Zhang), wanghuaisong@cpu.edu.cn, wanghuai1234@gmail.com (H.-S. Wang).

https://doi.org/10.1016/j.jpha.2022.05.007
2095-1779/

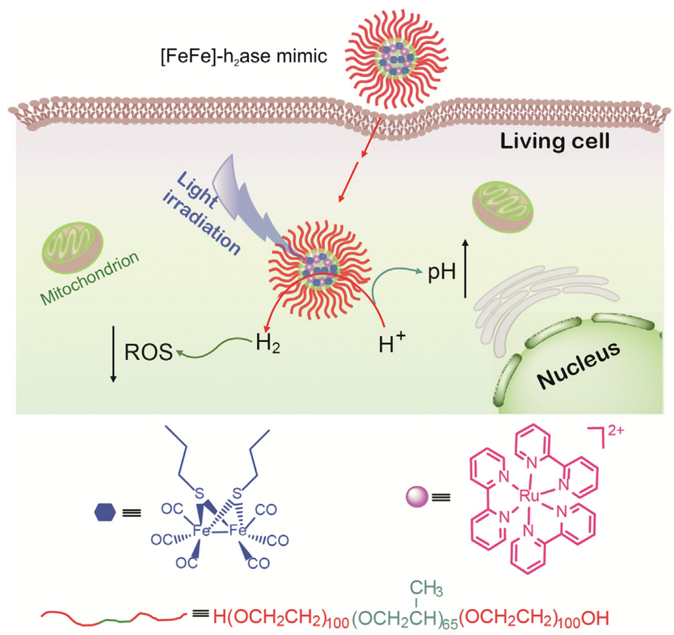

Fig. 1. [FeFe]-H_2ase nanoarchitecture (Ru + Fe_2S_2@F127) for moderating reactive oxygen species (ROS) and pH levels in living cancer cells.

cancer cells involved in the uptake of nanomaterials are slightly acidic [24,25]. In addition, the ROS levels in cancer cells are higher than those in healthy cells. Low pH and high oxidative stress may also damage healthy cells, resulting in their transformation into cancer cells and tumor aggravation. Inspired by the effective antioxidant ability of H_2, HeLa cells were used as a model to investigate the ROS and pH moderating ability of Ru + Fe_2S_2@F127 nanoarchitectures, which can be endocytosed into cancer cells. Under visible light, Ru + Fe_2S_2@F127 can photochemically reduce hydrated protons to H_2 and increase local pH. The generated H_2 was then used as an antioxidant to decrease ROS levels. The probes 2′,7′-dichlorodihydrofluorescein diacetate (DCHF-DA) and 2,7-bis(2-carboxyethyl)-5(6)-carboxyfluorescein tetrakis(acetoxymethyl) ester (BCECF-AM) were used to monitor intracellular ROS and pH levels, respectively. The imaging results show that this catalytic system provides a potential approach to increasing endogenous antioxidative protection and repairing the acid-base environment in living cells, especially in healthy cells around cancer tissues.

2. Materials and methods

2.1. Materials

Pluronic F-127, Ru(bpy)$_3$Cl$_2$, $Fe_3(CO)_{12}$, 1-propanethiol, and BCECF-AM were purchased from Sigma-Aldrich (St. Louis, MO, USA). MitoTracker Deep Red FM (MTDR) and 3-(4,5-dimethylthiazol-2-yl)-2,5-diphenyl-tetrazoliumbromide (MTT) were purchased from YEASEN (Shanghai, China). DCHF-DA was purchased from Sigma-Aldrich (St. Louis, MO, USA). Other reagents were purchased from Nanjing Chemical Reagent Co., Ltd. (Nanjing, China), and were of analytical grade. All aqueous solutions were prepared using deionized water (18 MΩ·cm; Pall Purelab Classic, New York City, NY, USA).

2.2. Instruments

The morphology of the Ru + Fe_2S_2@F127 nanoarchitecture was characterized using transmission electron microscopy (TEM; JEM-200CX, Tokyo, Japan). Fluorescence spectra were recorded using an RF-5301PC spectrophotometer (Shimadzu, Kyoto, Japan). Ultraviolet-visible (UV-vis) spectra were recorded on a UV-1800 spectrophotometer (Shimadzu, Kyoto, Japan). Fourier transform infrared (FT-IR) spectra were collected using a Bruker TENSOR 27 spectrometer (Bruker, Karlsruhe, Germany). Cell images were obtained using a TCS SP5 laser scanning confocal microscope (Leica, Heidelberg, Germany).

2.3. Methods

2.3.1. Synthesis of [Fe_2S_2] cluster (1-[Fe_2S_2])

Solid $Fe_3(CO)_{12}$ (100 mg, 0.2 mmol) and 1-propanethiol (36 μL, 0.4 mmol) were added to tetrahydrofuran (THF) (10 mL) under a N_2 atmosphere. The mixture was refluxed under N_2 for 2 h, and the color of the solution turned from dark green to red. The solvent was removed by vacuum evaporation, and the crude product was loaded onto a silica column (20 cm × 1.5 cm) and eluted with hexane to remove excess starting material. A red-orange crystalline product was obtained with a yield of approximately 70%. ^{1}H nuclear magnetic resonance (400 MHz, $CDCl_3$): δ2.7 (4H, m, SCH_2), δ1.7 (4H, m, $-CH_2-$), δ1.1 (6H, m, $-CH_3$). FT-IR (KBr): $\nu_{(-CH2-)} = 2928\ cm^{-1}$, $\nu_{(-CH3)} = 2971\ cm^{-1}$, $\nu_{(-C=O)} = 1984\ cm^{-1}$.

2.3.2. Synthesis of Ru + Fe_2S_2@F127

Pluronic F-127 (20, 40, and 80 mg), Ru(bpy)$_3$Cl$_2$ (1 mg), and 1-[Fe_2S_2] (1 mg) were dissolved in 0.6 mL of THF. After the THF was evaporated under vacuum, 1 mL of deionized water was added to the mixture, which was then stirred overnight at room temperature. The prepared Ru + Fe_2S_2@F127 micelles were collected by centrifugation at 9,000 r/min for 20 min and then re-dispersed in 1 mL of deionized water for the following experiment. The size of the Ru + Fe_2S_2@F127 micelles was characterized by TEM.

2.3.3. Photocatalytic hydrogen production

The Ru + Fe_2S_2@F127(80) suspension (100, 300, or 500 μL) was added to 5 mL of citrate buffer (50 mM, pH 4.5) containing 50 mM ascorbate. Before starting the photocatalytic experiment, the reaction mixture was purged with N_2 for 40 min. The sample was irradiated with light-emitting diodes (blue light, 50 W, λ = 400–480 nm). The generated H_2 was determined by gas chromatograph (GC) (Shimadzu GC2014, Kyoto, Japan) using a molecular sieve column (5 Å), loop size (3 mL), and a thermal conductivity detector.

2.3.4. Cell culture

HeLa, MCF-7, HepG2, and HEK 293T cells were cultured in Dulbecco's modified Eagle's medium supplemented with 10% fetal bovine serum (both from GIBCO, Grand Island, NY, USA), 5% penicillin streptomycin glutamine, and 5% sodium pyruvate at 37 °C in a humidified atmosphere containing 5% CO_2. Before the cell imaging experiments, HeLa cells were seeded in cell culture dishes and incubated for 24 h.

2.3.5. Intracellular ROS imaging

The Ru + Fe_2S_2@F127(80) suspension (20 μL) was added to cells in culture dishes, and the specimens were incubated for 30 min. After ·OH generation (Fenton reaction by 75 μM $FeCl_2$ + 150 μM H_2O_2 + 75 μM ethylenediamine tetraacetic acid (EDTA)) for 10 min, the cells were irradiated with light-emitting diodes (blue light, 50 W, λ = 400–480 nm) for 5 min or 10 min. The medium was removed, and the cells were washed with phosphate-buffered saline (PBS). Then MTDR (200 nM) was added, and the samples were incubated for 20 min, washed with PBS five

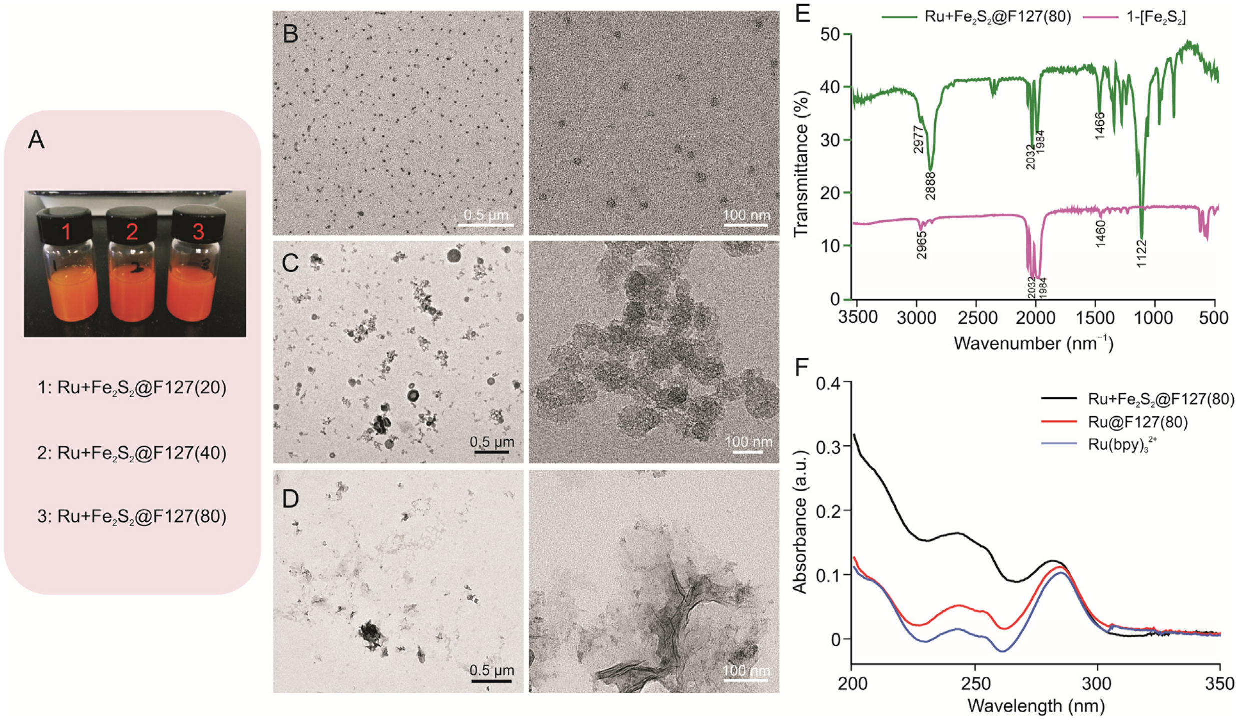

Fig. 2. Characterization of the Ru + Fe_2S_2@F127 nanoarchitectures. (A) Ru + Fe_2S_2@F127 nanoarchitecture dispersed in water; nanoparticles with increasing pluronic F-127 content: Ru + Fe_2S_2@F127(20), Ru + Fe_2S_2@F127(40), and Ru + Fe_2S_2@F127(80). Transmission electron microscopy (TEM) images of (B) Ru + Fe_2S_2@F127(80), (C) Ru + Fe_2S_2@F127(40), and (D) Ru + Fe_2S_2@F127(20). (E) Fourier transform infrared (FT-IR) spectra of Ru + Fe_2S_2@F127(80) and 1-[Fe_2S_2]. (F) Ultraviolet-visible (UV) absorbance spectra of Ru + Fe_2S_2@F127(80) and Ru@F127(80) and $Ru(bpy)_3^{2+}$.

times, and incubated with DCHF-DA (200 nM) for 30 min. After washing with PBS, confocal fluorescence imaging was performed.

2.3.6. Ethidium bromide/acridine orange (EB/AO) staining

The Ru + Fe_2S_2@F127(80) suspension (20 μL) was added to HeLa cell culture dishes and incubated for 30 min. Then, Fenton reagent (75 μM $FeCl_2$ + 150 μM H_2O_2 + 75 μM EDTA) was added and incubated for 10 min. HeLa cells were irradiated by light-emitting diodes (blue light, 50 W, $\lambda = 400–480$ nm) for 0, 2, 5, or 10 min. After 10 h, the cells were stained with EB/AO (100 μg/mL AO and 100 μg/mL EB) for 30 min for confocal fluorescence imaging.

2.3.7. Intracellular pH imaging

The Ru + Fe_2S_2@F127(80) suspension (20 μL) was added to cells in culture dishes, and the specimens were incubated for 30 min. The cells were irradiated by light-emitting diodes (blue light, 50 W, $\lambda = 400–480$ nm) for 10 min. BCECF-AM (250 nM) was then added, and the cells were incubated for 30 min. The cells were then washed with PBS prior to confocal fluorescence imaging.

2.3.8. Cell proliferation measurements

HeLa cells were seeded in six dishes and incubated under the same conditions for 24 h. Among the samples, one dish was treated with Fenton reagent as the control sample, and the other five dishes were treated with Ru + Fe_2S_2@F127(80) and ROS, generated by the Fenton reaction. HeLa cells in the five dishes that contained Ru + Fe_2S_2@F127(80) were irradiated with light-emitting diodes for 0, 2, 5, 10, and 14 min. The cells were then incubated for another 12 h and stained with AO solution (100 μg/mL) for 30 min. After washing with PBS, the living cells were counted using a fluorescent microscope.

3. Results and discussion

The active sites of mimics of [FeFe]-H_2ase for the chemical reduction of hydrated protons usually feature three central components: iron, thiolate groups, and carbon monoxide [26,27]. Combined with either electrochemical or photochemical reactions, improved catalytic performance of the [FeFe]-H_2ase mimics has been achieved [15,16,28]. In this study, an [Fe_2S_2] cluster (1-[Fe_2S_2]) was

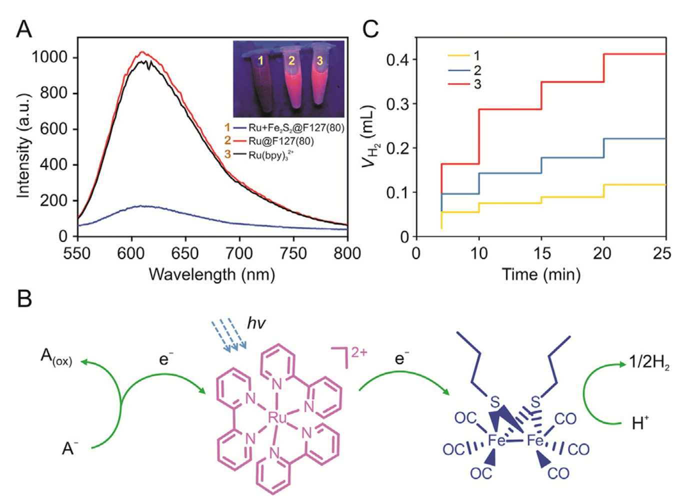

Fig. 3. Ru + Fe_2S_2@F127(80) nanoarchitectures for hydrogen production. (A) Fluorescence spectra of Ru + Fe_2S_2@F127(80), Ru@F127(80), and $Ru(bpy)_3^{2+}$ ($\lambda_{ex} = 470$ nm). The inset shows the visible fluorescence changes under irradiation with 365 nm light. (B) Reaction scheme for the photocatalytic reduction of hydrated protons to hydrogen. (C) Photocatalytic hydrogen production in the presence of different volumes of Ru + Fe_2S_2@F127(80) suspension. 1: 100 μL; 2: 300 μL; 3: 500 μL.

synthesized to mimic [FeFe]-H_2ase. As shown in Scheme S1, hydrophobic 1-[Fe_2S_2] was synthesized from $Fe_3(CO)_{12}$ and 1-propanethiol. $Ru(bpy)_3Cl_2$ was employed as a photosensitizer to supply the photogenerated electrons. To improve the photocatalytic efficiency for hydrogen evolution, a spatially confined nanoarchitecture of Ru + Fe_2S_2@F127 was synthesized by embedding 1-[Fe_2S_2] and $Ru(bpy)_3Cl_2$ into pluronic micelles containing $(PEO)_m(PPO)_n(PEO)_m$ (m = 100, n = 65, molecular weight = 12,600) [29–31]. A homogeneous mixture of 1-[Fe_2S_2], $Ru(bpy)_3Cl_2$, and pluronic F-127 in THF was first prepared. After adding water to the dried mixture, the triblock pluronic F-127 aggregated into micelles. Additionally, 1-[Fe_2S_2] and $Ru(bpy)_3Cl_2$ were incorporated into the hydrophobic PPO core.

Different weight ratios of pluronic F-127, $Ru(bpy)_3Cl_2$, and 1-[Fe_2S_2] (20:1:1, 40:1:1, and 80:1:1, respectively) were used to synthesize the Ru + Fe_2S_2@F127 nanoarchitectures. The three types of Ru + Fe_2S_2@F127 nanoarchitectures were denoted as Ru + Fe_2S_2@F127(20), Ru + Fe_2S_2@F127(40), and Ru + Fe_2S_2@F127(80), according to the proportion of pluronic F-127. As shown in Fig. 2A, all three types of Ru + Fe_2S_2@F127 were stably dispersed in water. However, the morphologies dramatically differed (Figs. 2B–D). The TEM images show that Ru + Fe_2S_2@F127(20) did not have a nanoparticle structure (Fig. 2D). With the increased pluronic F-127 concentration, a particulated Ru + Fe_2S_2@F127 nanostructure formed, and its size decreased with the increased pluronic F-127 concentration. Ru + Fe_2S_2@F127(80) showed a uniform particle size (approximately 10 nm), which was further applied in the study.

The composition of Ru + Fe_2S_2@F127(80) was investigated using FT-IR and UV spectroscopy (Figs. 2E, F, and S1). The UV spectrum of $Ru(bpy)_3^{2+}$ in Ru + Fe_2S_2@F127(80) was characterized by an absorption band of the bpy groups at 284 nm. The alkyl and alkoxy groups of 1-[Fe_2S_2] and pluronic F-127 showed strong absorption around 200 nm. The FT-IR spectrum of Ru + Fe_2S_2@F127(80) showed characteristic absorption bands of $\nu_{(-C=O)}$ = 1984 cm^{-1} from 1-[Fe_2S_2]. The absorption signal at 2977 cm^{-1} indicated the existence of $\nu_{(O-H)}$ in Ru + Fe_2S_2@F127(80), and the signal at approximately 2888 cm^{-1} is attributed to $\nu_{(C-H)}$.

The fluorescence emission properties of Ru + Fe_2S_2@F127(80) are shown in Fig. 3A. Ru@F127(80) was prepared using the same method as Ru + Fe_2S_2@F127(80), but without 1-[Fe_2S_2], and this sample was

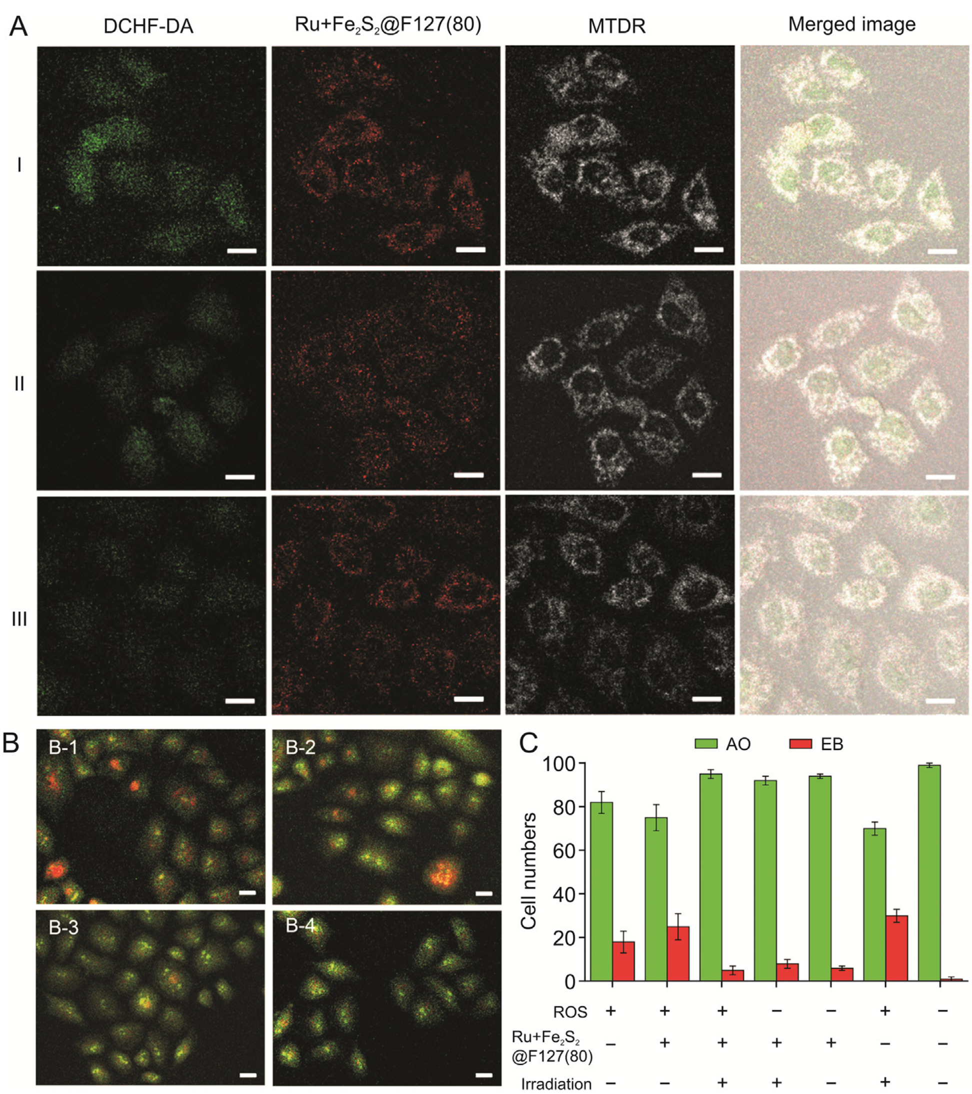

Fig. 4. Moderating reactive oxygen species (ROS) levels in Ru + Fe_2S_2@F127(80)-loaded HeLa cells. (A) Confocal images of intracellular ROS visualization after the cells were irradiated by blue light for 0 (I), 5 (II), and 10 min (III). Scale bar: 30 μm. (B) Confocal images of HeLa cells stained with ethidium bromide/acridine orange (EB/AO) after the cells were irradiated by blue light for 0 (B-1), 2 (B-2), 5 (B-3), and 10 min (B-4). Scale bar: 30 μm. (C) Numbers of EB- and AO-positive HeLa cells stained by EB/AO (the ROS was generated by Fenton reagent). The counted total cell number was 100 (n = 3). DCHF-DA: 2',7'-dichlorodihydrofluorescein diacetate; MTDR: MitoTracker Deep Red FM.

used as a control (Fig. S2). The fluorescence intensity of Ru + Fe_2S_2@F127(80) was significantly lower than that of Ru@F127(80), indicating that electron and/or energy transfer occurred from the photosensitizer ($Ru(bpy)_3^{2+}$) to the catalyst (1-[Fe_2S_2]), resulting in fluorescence quenching. The photocatalytic reduction of hydrated protons by Ru + Fe_2S_2@F127(80) commenced with the reductive quenching of photoexcited $Ru(bpy)_3^{2+}$. The electron transfer path during hydrogen generation is shown in Fig. 3B. By using ascorbate as an electron donor, the self-assembled system [Ru + Fe_2S_2@F127(80)] could produce H_2 under visible-light irradiation. As shown in Fig. S3, bubbles were clearly observed after light irradiation of the catalytic system. The generated H_2 was analyzed using GC. Fig. 3C shows that increasing the concentration of the Ru + Fe_2S_2@F127(80) catalyst and the irradiation time led to an obvious increase in H_2 evolution. In the absence of Ru + Fe_2S_2@F127(80), H_2 was not detected from the reaction system.

In nature, the H_2-generation activity of hydrogenases was first observed in *Escherichia coli*, from which the generated H_2 can be utilized to reduce a variety of substrates [32]. In this study, a hydrogenase mimic was, for the first time, introduced into human cancer cells for H_2 photogeneration, and successfully modulated intracellular ROS and pH levels. Ru + Fe_2S_2@F127(80) nanoarchitectures with a particle size of approximately 10 nm can be internalized by cells via clathrin-mediated endocytosis [33,34]. Subsequently, the cytotoxic effects of Ru + Fe_2S_2@F127(80) on HeLa cells after 48 h of incubation were studied using MTT assays (Fig. S4). The results showed slight cytotoxicity to HeLa cells when the concentration of Ru + Fe_2S_2@F127(80) reached 500 μg/mL, due to the high uptake of the nanoarchitectures into cells. The Ru + Fe_2S_2@F127(80)-loaded HeLa cells were further treated with blue light irradiation to catalyze intracellular hydrated proton reduction (Fig. S5). To monitor the changes in intracellular ROS levels, HeLa cells were incubated with Fenton reagent (approximately 0.15 mM) for 10 min before light irradiation [35,36]. Intracellular ROS levels were monitored by using DCHF-DA, which can be oxidized to dichlorofluorescein (DCF) by ROS. To observe the color change of DCF more accurately in living cells, the stable fluorescence intensity of MTDR (commercially available mitochondrial dye) was employed for comparison and colocalization. Fig. 4A shows that ROS-induced DCF was dispersed in the cytoplasm and nucleus. The fluorescence intensity of DCF was proportional to the amount of ROS in the cells. Without light irradiation, bright green fluorescence was observed in the HeLa cells, indicating high intracellular ROS levels. Under light irradiation, the green fluorescence intensity decreased in the Ru + Fe_2S_2@F127(80)-loaded HeLa cells, indicating that the photochemically generated H_2 reduced the ROS level in living cells. For comparison, Fenton reagent-treated HeLa cells were placed in a culture medium containing saturated molecular H_2 (Fig. S6). The results show that H_2 can reduce ROS levels, which is consistent with the findings of a previous report [8]. Although H_2 can be directly used to reduce ROS in living cells, it can potentially be degassed from the culture medium, resulting in an undesirable anti-ROS effect. Alternatively, H_2 generated by the Ru + Fe_2S_2@F127(80)

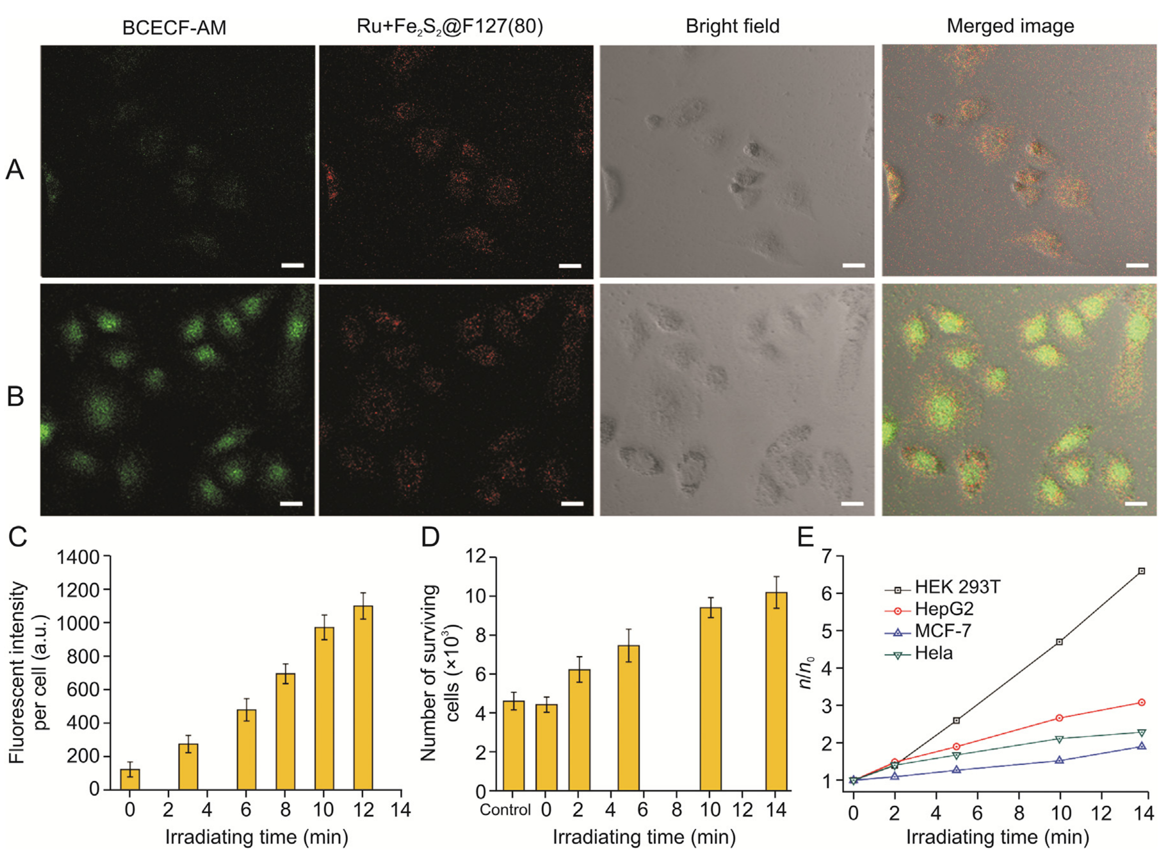

Fig. 5. Moderating pH levels in Ru + Fe_2S_2@F127(80)-loaded HeLa cells. Confocal images of intracellular pH measurements after cells were irradiated with blue light for (A) 0 and (B) 10 min. (C) 2,7-bis(2-carboxyethyl)-5(6)-carboxyfluorescein tetrakis(acetoxymethyl) ester (BCECF-AM) fluorescence was quantified from 100 cells of each independent experiment (n = 3). (D) Cell viability. After ROS treatment and light irradiation, living cells were counted in view in each well with a fluorescent microscope (n = 3). (E) Cell proliferation. The cells were treated with a Ru + Fe_2S_2@F127(80) suspension (20 μL) and Fenton reagent (75 μM $FeCl_2$ + 150 μM H_2O_2 + 75 μM ethylenediamine tetraacetic acid) and then irradiated by light-emitting diodes for 0–14 min. After the cells were incubated for 12 h, the number of the cells was recorded (n and n_0 are the numbers of surviving cells with and without light irradiation, respectively). Scale bar: 30 μm.

nanoarchitectures can be controlled by light irradiation time and intensity.

To investigate whether photocatalytic H_2 can protect cells from cell death caused by ROS, the EB/AO staining technique was employed to quantify cell viability. Fig. 4B shows the morphological features of Fenton-reagent-treated HeLa cells monitored using the EB/AO technique. With an increase in the light irradiation time, uniform green live cells with normal morphology were observed, which confirms that the photochemically generated H_2 can reduce the oxidative stress caused by ROS. Only under the conditions of Ru + Fe_2S_2@F127(80) and light irradiation were the ROS-treated cells protected (Fig. 4C).

The pH value of healthy cells is approximately 7.4, whereas tumor tissue exhibits acidic pH values that range from 5.7 to 7.8. Lower pH values, in the range from 4.5 to 5.5, can be found at the subcellular level, such as in late endosomes and lysosomes [37,38]. Under visible light, the Ru + Fe_2S_2@F127(80) nanoarchitecture reduced hydrated protons to H_2 in HeLa cells. This may increase the pH of HeLa cells; thus, to monitor intracellular pH changes after H_2 generation, the pH-sensitive dye BCECF-AM was used as a local pH probe. Figs. 5A and B shows that the fluorescence intensity increased in Ru + Fe_2S_2@F127(80)-loaded HeLa cells after light irradiation. Furthermore, with the increased irradiation time, the intracellular fluorescence intensity increased accordingly (Fig. 5C), indicating that hydrated protons were consumed by Ru + Fe_2S_2@F127(80) during the light irradiation. The slight fluorescence of BCECF-AM was also observed in cells without irradiation (Fig. S7). After light irradiation, the obvious increase in fluorescence intensity indicated the successful reduction of hydrated protons by Ru + Fe_2S_2@F127(80). The extracellular experiment also proved that the increase in pH was due to the reduction of hydrated protons to H_2 by Ru + Fe_2S_2@F127(80) (Fig. S8). After light irradiation for 10 min, the pH changed from 3.8 to 6.2.

Considering that excessive ROS and an unusual pH environment may cause cellular damage and various diseases, cell viability was investigated before and after moderating the ROS and pH levels. HeLa cells were first treated with the Fenton reagent. The Ru + Fe_2S_2@F127(80) nanoarchitectures were then incubated with HeLa cells. As shown in Fig. 5D, with different light irradiation time, the generated H_2 increased cell survival and vitality, indicating that H_2 protected the cells against ROS and/or pH-induced cell death. This phenomenon was also observed in other living cells (Fig. 5E). In particular, light irradiation treatment had the most obvious effect on the survival of HEK 293T cells compared with the other cells, including HepG2, MCF-7, and HeLa cells. After light irradiation, the number of surviving HEK 293T cells was six times larger than that of surviving cells in the absence of light irradiation. This may be because HEK 293T cells are most sensitive to ROS stress, resulting in a low cell survival ratio under ROS treatment. However, after light irradiation, cell death was suppressed due to H_2 generation. This shows that the Ru + Fe_2S_2@F127(80) nanoarchitecture can protect healthy cells from oxidative stress and potentially control the deterioration of tumors.

4. Conclusion

In summary, we developed a type of [FeFe]-H_2ase mimic, Ru + Fe_2S_2@F127(80), for H_2 photogeneration in living cells that was capable of moderating intracellular ROS and pH levels, which were evaluated using fluorescent cell imaging methods. The Ru + Fe_2S_2@F127(80) nanoarchitecture can be self-assembled by biocompatible polymeric pluronic F-127, catalytic [Fe_2S_2] sites, and photosensitizer $Ru(bpy)_3^{2+}$. In Ru + Fe_2S_2@F127(80)-loaded living cells, blue light irradiation could locally promote the reduction of hydrated protons to H_2, which can function as an antioxidant to decrease ROS levels, accompanied by an increase in pH. Notably, the generated H_2 can increase cell survival and vitality. In summary, our study shows that Ru + Fe_2S_2@F127(80) can potentially be used to prevent the aggravation and deterioration of tumors caused by oxidative damage to healthy cells.

CRediT author statement

Xin-Yuan Hu: Investigation, Formal analysis, Writing - Original draft preparation; **Jia-Jing Li**: Validation, Writing - Original draft preparation; **Zi-Wei Yang**: Validation, Writing - Original draft preparation; **Jun Zhang**: Methodology, Visualization; **Huai-Song Wang**: Conceptualization, Supervision, Writing - Reviewing and Editing.

Declaration of competing interest

The authors declare that there are no conflicts of interest.

Acknowledgments

This work was supported by the National Natural Science Foundation of China (Grant No.: 21705165), the Open Project Program of the MOE Key Laboratory of Drug Quality Control and Pharmacovigilance (Grant No.: DQCP20/21MS03), the Priority Academic Program Development of Jiangsu Higher Education Institutions, and "Double First-Class" University Project (Grant No.: CPU2018GF07).

Appendix A. Supplementary data

Supplementary data to this article can be found online at https://doi.org/10.1016/j.jpha.2022.05.007.

References

[1] B.W. Yang, Y. Chen, J.L. Shi, Reactive oxygen species (ROS)-based nanomedicine, Chem. Rev. 119 (2019) 4881–4985.
[2] M. Lian, Z. Xue, X. Qiao, et al., Movable hollow nanoparticles as reactive oxygen scavengers, Inside Chem. 5 (2019) 2378–2387.
[3] L. Wang, B. Zhu, Y. Deng, et al., Biocatalytic and antioxidant nanostructures for ROS scavenging and biotherapeutics, Adv. Funct. Mater. 31 (2021), 2101804.
[4] M. Chen, L. Jiang, Y. Li, et al., Hydrogen protects against liver injury during CO_2 pneumoperitoneum in rats, Oncotarget 9 (2017) 2631–2645.
[5] F. Xu, S. Yu, M. Qin, et al., Hydrogen-rich saline ameliorates allergic rhinitis by reversing the imbalance of Th1/Th2 and up-regulation of CD4+CD25+Foxp3+regulatory T cells, interleukin-10, and membrane-bound transforming growth factor-β in Guinea pigs, Inflammation 41 (2018) 81–92.
[6] L.C. Chen, S.F. Zhou, L.C. Su, et al., Gas-mediated cancer bioimaging and therapy, ACS Nano 13 (2019) 10887–10917.
[7] Y. Gao, Q. Gui, L. Jin, et al., Hydrogen-rich saline attenuates hippocampus endoplasmic reticulum stress after cardiac arrest in rats, Neurosci. Lett. 640 (2017) 29–36.
[8] I. Ohsawa, M. Ishikawa, K. Takahashi, et al., Hydrogen acts as a therapeutic antioxidant by selectively reducing cytotoxic oxygen radicals, Nat. Med. 13 (2007) 688–694.
[9] L. Ge, M. Yang, N.N. Yang, et al., Molecular hydrogen: A preventive and therapeutic medical gas for various diseases, Oncotarget 8 (2017) 102653–102673.
[10] L. Yao, H. Chen, Q. Wu, et al., Hydrogen-rich saline alleviates inflammation and apoptosis in myocardial I/R injury via PINK-mediated autophagy, Int. J. Mol. Med. 44 (2019) 1048–1062.
[11] Z. Zhang, X. Sun, K. Wang, et al., Hydrogen-saturated saline mediated neuroprotection through autophagy via PI3K/AKT/mTOR pathway in early and medium stages of rotenone-induced Parkinson's disease rats, Brain Res. Bull. 172 (2021) 1–13.
[12] K. Li, H.L. Yin, Y. Duan, et al., Pre-inhalation of hydrogen-rich gases protect against caerulein-induced mouse acute pancreatitis while enhance the pancreatic Hsp60 protein expression, BMC Gastroenterol. 21 (2021), 178.
[13] Q. Shi, K. Liao, K. Zhao, et al., Hydrogen-rich saline attenuates acute renal injury in sodium taurocholate-induced severe acute pancreatitis by inhibiting ROS and NF-κB pathway, Mediat. Inflamm. 2015 (2015), 685043.
[14] M.A. Martini, O. Rüdiger, N. Breuer, et al., The nonphysiological reductant sodium dithionite and [FeFe] hydrogenase: Influence on the enzyme mechanism, J. Am. Chem. Soc. 143 (2021) 18159–18171.

[15] J. Jian, Q. Liu, Z. Li, et al., Chitosan confinement enhances hydrogen photogeneration from a mimic of the diiron subsite of [FeFe]-hydrogenase, Nat. Commun. 4 (2013), 2695.
[16] S. Pullen, H. Fei, A. Orthaber, et al., Enhanced photochemical hydrogen production by a molecular diiron catalyst incorporated into a metal-organic framework, J. Am. Chem. Soc. 135 (2013) 16997–17003.
[17] A. Roy, C. Madden, G. Ghirlanda, Photo-induced hydrogen production in a helical peptide incorporating a [FeFe] hydrogenase active site mimic, Chem. Commun. 48 (2012) 9816–9818.
[18] S. Ott, M. Kritikos, B. Åkermark, et al., Synthesis and structure of a biomimetic model of the iron hydrogenase active site covalently linked to a ruthenium photosensitizer, Angew. Chem., Int. Ed. Engl. 42 (2003) 3285–3288.
[19] M. Wen, X. Li, J. Jian, et al., Secondary coordination sphere accelerates hole transfer for enhanced hydrogen photogeneration from [FeFe]-hydrogenase mimic and CdSe QDs in water, Sci. Rep. 6 (2016), 29851.
[20] J.X. Jian, C. Ye, X.Z. Wang, et al., Comparison of H_2 photogeneration by [FeFe]-hydrogenase mimics with CdSe QDs and $Ru(bpy)_3Cl_2$ in aqueous solution, Energy Environ. Sci. 9 (2016) 2083–2089.
[21] H.-Q. Zheng, X.-B. Wang, J.-Y. Hu, et al., Photo-catalytic H_2 evolution, structural effect and electron transfer mechanism based on four novel [2Fe2S] model complexes by photochemical splitting water, Sol. Energy 132 (2016) 373–385.
[22] Y.D. Lee, C.K. Lim, A. Singh, et al., Dye/peroxalate aggregated nanoparticles with enhanced and tunable chemiluminescence for biomedical imaging of hydrogen peroxide, ACS Nano 6 (2012) 6759–6766.
[23] C.-K. Lim, Y.-D. Lee, J. Na, et al., Chemiluminescence-generating nanoreactor formulation for near-infrared imaging of hydrogen peroxide and glucose level *in vivo*, Adv. Funct. Mater. 20 (2010) 2644–2648.
[24] Z. Zhao, X. Yao, Z. Zhang, et al., Boronic acid shell-crosslinked dextran-b-PLA micelles for acid-responsive drug delivery, Macromol. Biosci. 14 (2014) 1609–1618.
[25] K. Yang, H. Luo, M. Zeng, et al., Intracellular pH-triggered, targeted drug delivery to cancer cells by multifunctional envelope-type mesoporous silica nanocontainers, ACS Appl. Mater. Interfaces 7 (2015) 17399–17407.
[26] D. Sil, Z. Martinez, S. Ding, et al., Cyanide docking and linkage isomerism in models for the artificial [FeFe]-hydrogenase maturation process, J. Am. Chem. Soc. 140 (2018) 9904–9911.
[27] M.E. Ahmed, S. Dey, M.Y. Darensbourg, et al., Oxygen-tolerant H_2 production by [FeFe]-H_2ase active site mimics aided by second sphere proton shuttle, J. Am. Chem. Soc. 140 (2018) 12457–12468.
[28] D. Schilter, T.B. Rauchfuss, And the winner is...azadithiolate: An amine proton relay in the [FeFe] hydrogenases, Angew. Chem., Int. Ed. Engl. 52 (2013) 13518–13520.
[29] U. Anand, S. Mukherjee, Microheterogeneity and microviscosity of F127 micelle: The counter effects of urea and temperature, Langmuir 30 (2014) 1012–1021.
[30] M. Valero, F. Castiglione, A. Mele, et al., Competitive and synergistic interactions between polymer micelles, drugs, and cyclodextrins: The importance of drug solubilization locus, Langmuir 32 (2016) 13174–13186.
[31] Z. Yang, Y. Zhang, J. Kong, et al., Hollow carbon nanoparticles of tunable size and wall thickness by hydrothermal treatment of α-cyclodextrin templated by F127 block copolymers, Chem. Mater. 25 (2013) 704–710.
[32] M. Stephenson, L.H. Stickland, Hydrogenase: A bacterial enzyme activating molecular hydrogen: The properties of the enzyme, Biochem. J. 25 (1931) 205–214.
[33] H. Herd, N. Daum, A.T. Jones, et al., Nanoparticle geometry and surface orientation influence mode of cellular uptake, ACS Nano 7 (2013) 1961–1973.
[34] J. Rejman, V. Oberle, I.S. Zuhorn, et al., Size-dependent internalization of particles via the pathways of clathrin-and caveolae-mediated endocytosis, Biochem. J. 377 (2004) 159–169.
[35] S. Liu, J. Zhao, K. Zhang, et al., Dual-emissive fluorescence measurements of hydroxyl radicals using a coumarin-activated silica nanohybrid probe, Analyst 141 (2016) 2296–2302.
[36] L. Meng, Y. Wu, T. Yi, A ratiometric fluorescent probe for the detection of hydroxyl radicals in living cells, Chem. Commun. 50 (2014) 4843–4845.
[37] K. Engin, D.B. Leeper, J.R. Cater, et al., Extracellular pH distribution in human tumours, Int. J. Hyperther. 11 (1995) 211–216.
[38] M. Stubbs, P.M. McSheehy, J.R. Griffiths, et al., Causes and consequences of tumour acidity and implications for treatment, Mol. Med. Today 6 (2000) 15–19.